Full length article

Study of the asymptotic Cramér–Rao Bound for the COLD uniform linear array

Rémy Boyer [a,1], Sebastian Miron [b,*]

[a] Laboratoire des Signaux et Systemes (CNRS - Université Paris-Sud - Supélec) 3, rue Joliot-Curie, 91190, Gif-sur-Yvette, France
[b] Centre de Recherche en Automatique de Nancy, Nancy-Université, CNRS, Boulevard des Aiguillettes, B.P. 239, F-54506 Vandœuvre-lès-Nancy, France

ARTICLE INFO

ABSTRACT

In this paper, we study the Cocentered Orthogonal Loop and Dipole pairs Uniform Linear Array (COLD-ULA) which is sensitive to the source polarization in the context of the localization of time-varying narrow-band far-field sources. We derive and analyze nonmatrix expressions of the deterministic Cramér–Rao Bound ($CRB^{(COLD)}$) for the direction and the polarization parameters under the assumption that all the sources are lying in the azimuthal plane. We denote this bound by $ACRB^{(COLD)}$, where the "A" stands for Asymptotic, meaning that the presented results are derived under the assumption that the number of sensors is sufficiently large. While, to our knowledge, closed-form (nonmatrix) expressions of the $CRB^{(COLD)}$ for multiple time-varying polarized sources signal do not exist in the literature, we show that the $ACRB^{(COLD)}$ takes a closed-form (nonmatrix) expression in this context and is a good approximation of the $CRB^{(COLD)}$ even if the number of sensor is moderate (about ten), if the source signals are not spatially too close. Our approach has two important advantages: (i) the computational complexity of the proposed closed-form of the bound is very low, compared to the brute force computation of a matrix-based deterministic CRB in case of time-varying model parameters and (ii) useful informations can be deduced from the closed-form expression on the behavior of the bound. In particular, we prove that the $ACRB^{(COLD)}$ for the direction parameter is not affected by the knowledge or the lack of it concerning the polarization parameters. Another conclusion is that with a COLD-ULA, more model parameters can be estimated than for the uniformly polarized ULA without degrading the estimation accuracy of the localization parameter. Finally, we also study the $ACRB^{(COLD)}$ for *a priori* known complex amplitudes.

© 2012 Elsevier B.V. All rights reserved.

1. Introduction

Wireless communication systems, including cellular radio, need to operate in increasingly more crowded signal environments. Antenna arrays provide an important capability for separating multiple superimposed communication signals. In this context, polarization diversity along with the spatial diversity has become an important parameter in a wireless communication system. In the localization of narrowband far-field polarized sources context, we can find plethora of estimation methods. In [1], the Maximum Likelihood Estimator (MLE) for diversely polarized source localization was proposed. In [2–5], the ESPRIT algorithm using vector sensors has been investigated. Another scheme based on a shift-invariance property is proposed in [6]. MUSIC-based algorithms for this problem have been applied in [7,8] while another approach, based on the MODE algorithm, was introduced in [9]. In [10], the interest of crossed-dipole array is demonstrated for asynchronous DS-CDMA systems and for seismic processing in [11]. In [12], a MUSIC algorithm based on the Higher-Order Statistics is presented, and in [13,14] hypercomplex algebra is used to deal with vector sensor array data.

* Corresponding author. Tel.: +33 3 83 68 44 69; fax: +33 3 83 68 44 62.
E-mail addresses: remy.boyer@lss.supelec.fr (R. Boyer), sebastian.miron@cran.uhp-nancy.fr (S. Miron).
1 Tel.: +33 1 69 85 17 12; fax: +33 1 69 85 17 69.

Identifiability and uniqueness issues associated with the considered model are analyzed in [15–17]. The resolution limit has been derived and analyzed in Ref. [18]. In [19–21], we can find the *matrix-based* expression of the Cramér–Rao Bound (CRB) for the considered model and in [22], the authors derive and study closed-form (nonmatrix) expressions of the bound for known polarization state and for a known single source. Remark that the assumption of known model parameters leads to optimistic lower bounds [23]. We can find in the literature (*e.g.* [24,25]) the deterministic and the stochastic CRB. In the first case, considered in this paper, the sources are assumed to be unknown deterministic while in the stochastic case, they are viewed as unknown Gaussian random variables. The deterministic CRB is important since we know that for sufficient Signal-to-Noise-Ratio the MLE meets this bound [26]. As a consequence, this bound is widely used as a benchmark to evaluate suboptimal estimator (regarding the MLE). However, the difficult point with the deterministic CRB is that the number of source parameters grows with the number of snapshots. This implies the inversion of a large Fisher Information Matrix (FIM) and thus a large computational cost. We can find in [27–29], closed-forms expression of the deterministic CRB but to the best of our knowledge, this bound for multiple unknown far-field time-varying[2] narrowband polarized sources has not been sufficiently investigated.

In this paper, we derive and analyze nonmatrix (closed-form) expressions of the deterministic CRB for multiple unknown far-field time-varying narrowband polarized sources, impinging a Cocentered Orthogonal Loop and Dipole pairs Uniform Linear Array (COLD-ULA) [9]. For simplification we assume that all the sources are localized in the azimuthal plane (*i.e.* their elevation angle equals $\pi/2$). This corresponds, for example, to a scenario where all the polarized sources are localized at ground level. In order to obtain a nonmatrix expression of the CRB we use the theoretical assumption that the number of sensors tends to infinity, leading to the "Asymptotic" CRB (ACRB). At first glance, this assumption seems severe but we show numerically that the ACRB closely approximates the CRB, even for small/moderate number of sensors and for sufficiently spaced sources. This has already been noticed in context of training sequence design [30] for instance. Nonmatrix expressions of the CRB [31,32,22] are important for at least two reasons: (i) the computation of these expressions is very cheap while the brute force inversion of the FIM can be a cumbersome task in case of time-varying model parameters and (ii) they provide useful informations on the behavior of the bound since they depend explicitly and clearly on the model parameters.

The paper is organized as follow. Section 2 presents the model of the signal observed on the COLD-ULA. The matrix-based deterministic CRB for the COLD-ULA is introduced in Section 3. Section 4 is dedicated to the definition and the
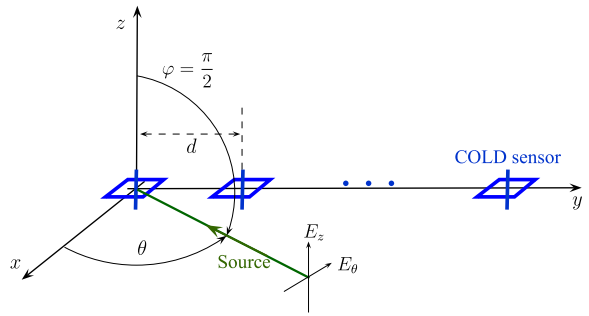
Fig. 1. Acquisition scheme with the COLD-ULA array.
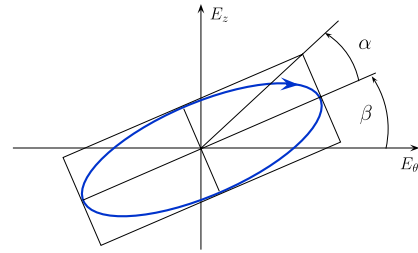
Fig. 2. Polarization ellipse.

derivation of the closed-form (nonmatrix) Asymptotic CRB for the COLD-ULA regarding the direction and polarization parameters. Next, Section 5 presents the analysis of this bound and introduces some comparisons. Numerical validations and illustrations of the proposed nonmatrix expressions of the bound are given in Section 6. Section 7 provides some concluding remarks.

2. Model of the signal received on a Cocentered Orthogonal Loop and Dipole pairs Uniform Linear Array (COLD-ULA)

Consider a uniform linear array consisting of L COLD pairs, two successive pairs being separated by a distance d, as shown in Fig. 1. The array is collinear with the *y*-axis of a *Oxyz* coordinate system with its origin in the center of the first pair of sensors. For each COLD pair, the dipole is parallel to the *z*-axis and the loop is parallel to the *x–y* plane.

Assume M narrowband far-field plane waves impinge on the array from directions described by the *elevation* angle φ and *azimuth* angle θ. In this paper we suppose that all the sources are contained in the *x–y* azimuthal plane, *i.e.* $\varphi = \frac{\pi}{2}$, as illustrated in Fig. 1. Furthermore, suppose each signal is a completely polarized transverse electromagnetic wave, with an elliptical polarization of *ellipticity* α ($-\frac{\pi}{4} \leq \alpha \leq \frac{\pi}{4}$) and *orientation* β ($0 \leq \beta < \pi$) (see Fig. 2). For a given signal polarization, the vertical and the horizontal components (E_z and E_θ) of the incoming signal electric field E can be specified by polarization constants ρ and ψ [33,9] as

$$E_\theta = E \cos \rho, \tag{1}$$

$$E_z = E \sin \rho \exp(i\psi). \tag{2}$$

The values of ρ ($0 \leq \rho \leq \frac{\pi}{2}$) and ψ ($-\pi \leq \psi < \pi$) can be used to compute the polarization ellipse parameters α

---

[2] Note that the proposed source signal model is different to the one in Ref. [28]. In particular, the number of parameters of interest in our contribution grows with the number of snapshots. This is not the case in [28,29]. This technical difference is important regarding the complexity cost of the FIM inversion.

and β [34,35]. For example, $\psi = 0$ implies $\alpha = 0$, which means (see Fig. 2) that the source is linearly polarized. A zero value of ρ implies $\alpha = 0$ and $\beta = 0$ meaning that the source polarization is linear horizontal, while if $\rho = \frac{\pi}{2}$, then $\beta = \frac{\pi}{2}$ and $\alpha = 0$, *i.e.* the polarization is linear vertical. These remarks will be used in the following sections to facilitate the interpretation of the CRB results.

2.1. The model of the polarized source mixture recorded on a single COLD pair

Under the given assumptions, the output of the ℓ-th pair of the COLD-ULA represented in Fig. 1 can be expressed by [9,35]

$$\bar{\boldsymbol{x}}_\ell(t) = \begin{bmatrix} x_\ell(t) \\ y_\ell(t) \end{bmatrix} = \sum_{m=1}^{M} \alpha_m(t) \boldsymbol{u}_m z_m^\ell \tag{3}$$

in which $x_\ell(t)$ and $y_\ell(t)$ are the signals recorded on the small loop and short dipole, respectively. In (3), $z_m = e^{i\frac{2\pi}{\lambda} d \sin(\theta_m)}$ is the phase factor for the mth source, with λ the wavelength. The time-varying sources are modeled by $\alpha_m(t) = a_m e^{i(2\pi f_0 t + \phi_m(t))}$, where a_m is the non-zero real amplitude, $\phi_m(t)$ is the time-varying modulating phase and f_0 is the carrier frequency of the incident wave. $\boldsymbol{u}_m$ is the 2×1 polarization state vector given by

$$\boldsymbol{u}_m = \begin{bmatrix} \dfrac{2i\pi A_{sl}}{\lambda} \cos(\rho_m) \\ -L_{sd} \sin(\rho_m) e^{i\psi_m} \end{bmatrix} \tag{4}$$

where L_{sd} and A_{sl} represent the length of the short dipole and the area of the small loop. In (4) we used the fact that for short dipoles and small loops the output voltages are proportional to the electric field components parallel to dipole and loop, respectively. Note that, from a modeling point of view, we can assume $L_{sd} = \frac{2\pi A_{sl}}{\lambda} = 1$.

The COLD polarization state vector presents several interesting properties listed below:

P1. $\partial \boldsymbol{u}_m / \partial \theta_m = \boldsymbol{0}$, *i.e.* the polarization state vector of a COLD array is not a function of the direction parameter.
P2. $\|\boldsymbol{u}_m\|^2 = 1$, *i.e.* the norm of the polarization state vector is one.
P3. $\|\partial \boldsymbol{u}_m / \partial \rho_m\|^2 = 1$, *i.e.* the norm of the differentiation of the polarization state vector with respect to parameter ρ_m is one.
P4. $\boldsymbol{u}_m$ and $\partial \boldsymbol{u}_m / \partial \rho_m$ are orthogonal, *i.e.* $\langle \boldsymbol{u}_m, \partial \boldsymbol{u}_m / \partial \rho_m \rangle = 0$ where $\langle ., . \rangle$ stands for the Hermitian inner product.
P5. $\|\partial \boldsymbol{u}_m / \partial \psi_m\|^2 = \sin^2(\rho_m)$, *i.e.* the norm of the differentiation of the polarization state vector with respect to parameter ψ_m is simply a trigonometric function of parameter ρ_m. We have $\|\partial \boldsymbol{u}_m / \partial \psi_m\|^2 \leq 1$.
P6. $\langle \boldsymbol{u}_m, \partial \boldsymbol{u}_m / \partial \psi_m \rangle = i \|\partial \boldsymbol{u}_m / \partial \psi_m\|^2$, meaning that the Hermitian inner product between the polarization state vector and its differentiation with respect to parameter ψ_m is a pure imaginary quantity, linked to the norm of the differentiation of the polarization state vector with respect to parameter ψ_m.

2.2. The space-time model of the data recorded on a COLD-ULA

Let us now define the $2L \times 1$ vector collecting the observation over the L sensor pairs of the array, according to

$$\check{\boldsymbol{x}}(t) = \begin{bmatrix} \bar{\boldsymbol{x}}_0(t) \\ \vdots \\ \bar{\boldsymbol{x}}_{L-1}(t) \end{bmatrix} = \sum_{m=1}^{M} \boldsymbol{A}_m(t) \boldsymbol{d}_m \tag{5}$$

where $\boldsymbol{A}_m(t) = \boldsymbol{I}_L \otimes (\alpha_m(t) \boldsymbol{u}_m)$ is of size $(2L) \times L$. Operator $\otimes$ stands for the Kronecker product and the steering vector is defined by

$$\boldsymbol{d}_m = \begin{bmatrix} 1 & e^{i\frac{2\pi}{\lambda} d \sin(\theta_m)} & \cdots & e^{i(L-1)\frac{2\pi}{\lambda} d \sin(\theta_m)} \end{bmatrix}^T$$

where the superscript $(.)^T$ denotes the transposition operator. Collecting the above observation for T snapshots, the final noise corrupted $(2LT) \times 1$ vector model is

$$\boldsymbol{y} = \check{\boldsymbol{x}} + \sigma \boldsymbol{e} \tag{6}$$

where

$$\check{\boldsymbol{x}} = \begin{bmatrix} \check{\boldsymbol{x}}(1) \\ \vdots \\ \check{\boldsymbol{x}}(T) \end{bmatrix} = \sum_{m=1}^{M} \begin{bmatrix} \boldsymbol{A}_m(1) \boldsymbol{d}_m \\ \vdots \\ \boldsymbol{A}_m(T) \boldsymbol{d}_m \end{bmatrix}$$

and $\boldsymbol{e}$ is an additive white circular complex centered (zero-mean) Gaussian noise of covariance $\boldsymbol{I}_{2LT}$.

3. Deterministic Cramér–Rao Bound for the COLD-ULA

The noisy observation $\boldsymbol{y}$ in expression (6) is constituted by the deterministic signal of interest corrupted by a complex Gaussian noise. So, the observation $\boldsymbol{y}$ follows a Gaussian distribution such as $\boldsymbol{y} \sim \mathcal{CN}(\check{\boldsymbol{x}}, \sigma^2 \boldsymbol{I}_{2LT})$ and is a function of the real deterministic unknown parameter vector $\boldsymbol{\varepsilon}$ given by $\boldsymbol{\varepsilon} = [\boldsymbol{\varepsilon}'^T \ \sigma^2]^T$ in which the noise power σ^2 is an unknown and unwanted (nuisance) parameter and

$$\boldsymbol{\varepsilon}' = \begin{bmatrix} \underline{\theta}^T & \underline{\psi}^T & \underline{\phi}^T & \underline{\rho}^T & \underline{a}^T \end{bmatrix}^T \tag{7}$$

where $\underline{a} = [a_1 \cdots a_M]^T$, $\underline{\rho} = [\rho_1 \cdots \rho_M]^T$, $\underline{\phi} = [\underline{\phi}(1)^T \cdots \underline{\phi}(T)^T]^T$ with $\underline{\phi}(t) = [\phi_1(t) \cdots \phi_M(t)]^T$, $\underline{\psi} = [\psi_1 \cdots \psi_M]^T$, $\underline{\theta} = [\theta_1 \cdots \theta_M]^T$, are the parameters of interest.

A fundamental result (*e.g.* [36,37,24]) is the following. Let $E\{(\hat{\boldsymbol{\varepsilon}} - \boldsymbol{\varepsilon})(\hat{\boldsymbol{\varepsilon}} - \boldsymbol{\varepsilon})^T\}$ be the covariance matrix of an (locally) unbiased estimate of $\boldsymbol{\varepsilon}$, denoted by $\hat{\boldsymbol{\varepsilon}}$ and define the deterministic Cramér–Rao Bound (CRB) dedicated to the COLD-ULA, denoted by CRB$^{(\text{COLD})}$. The covariance inequality principle states that under quite general/weak conditions, we have MSE$([\hat{\boldsymbol{\varepsilon}}]_i) = E\{([\hat{\boldsymbol{\varepsilon}}]_i - [\boldsymbol{\varepsilon}]_i)^2\} \geq$ CRB$^{(\text{COLD})}([\boldsymbol{\varepsilon}]_i)$, for $i \in [1 : (T+4)M+1]$. More specifically, the deterministic CRB *wrt.* the signal parameters, $\boldsymbol{\varepsilon}'$, is given by

$$\text{CRB}^{(\text{COLD})}([\boldsymbol{\varepsilon}']_i) = \frac{\sigma^2}{2} \left[\boldsymbol{F}_{\boldsymbol{\varepsilon}'\boldsymbol{\varepsilon}'}^{-1} \right]_{ii}, \quad \text{for } i \in [1 : (T+4)M] \tag{8}$$

and

$$\boldsymbol{F_{\varepsilon'\varepsilon'}} = \begin{bmatrix} \boldsymbol{J_{\underline{\theta\theta}}} & \boldsymbol{J_{\underline{\theta\psi}}} & \boldsymbol{J_{\underline{\theta\phi}}} & \boldsymbol{J_{\underline{\theta\rho}}} & \boldsymbol{J_{\underline{\theta a}}} \\ \boldsymbol{J_{\underline{\theta\psi}}^T} & \boldsymbol{J_{\underline{\psi\psi}}} & \boldsymbol{J_{\underline{\psi\phi}}} & \boldsymbol{J_{\underline{\psi\rho}}} & \boldsymbol{J_{\underline{\psi a}}} \\ \boldsymbol{J_{\underline{\theta\phi}}^T} & \boldsymbol{J_{\underline{\psi\phi}}^T} & \boldsymbol{J_{\underline{\phi\phi}}} & \boldsymbol{J_{\underline{\phi\rho}}} & \boldsymbol{J_{\underline{\phi a}}} \\ \boldsymbol{J_{\underline{\theta\rho}}^T} & \boldsymbol{J_{\underline{\psi\phi}}^T} & \boldsymbol{J_{\underline{\phi\rho}}^T} & \boldsymbol{J_{\underline{\rho\rho}}} & \boldsymbol{J_{\underline{\rho a}}} \\ \boldsymbol{J_{\underline{\theta a}}^T} & \boldsymbol{J_{\underline{\psi a}}^T} & \boldsymbol{J_{\underline{\phi a}}^T} & \boldsymbol{J_{\underline{\rho a}}^T} & \boldsymbol{J_{\underline{aa}}} \end{bmatrix} \tag{9}$$

is the $(M(T+4)) \times (M(T+4))$ Fisher Information Matrix (FIM) *wrt.* the signal parameter $\boldsymbol{\varepsilon}'$. In addition, in (9) we have defined each block of the FIM by

$$[\boldsymbol{J_{\underline{pq}}}]_{ij} = \Re \left\{ \left(\frac{\partial \boldsymbol{\check{x}}}{\partial [\underline{p}]_i} \right)^H \frac{\partial \boldsymbol{\check{x}}}{\partial [\underline{q}]_j} \right\} \tag{10}$$

with $(.)^H$ being the conjugate-transpose operator, $\Re\{.\}$ being the real part of a complex number and $\boldsymbol{\check{x}}$ is the noise-free model introduced in expression (5). Note that to obtain (8), we have exploited the well-known property that the signal and the nuisance (noise variance) parameters are decoupled. So, the CRB for the i-th signal parameter, denoted by $[\boldsymbol{\varepsilon}']_i$, is given by the (i, i)-th term of the inverse of the FIM weighed by $\sigma^2/2$. Note that in the case of the deterministic CRB, we need to inverse a FIM of size growing with T. So for large T, this operation may have a high computational cost.

4. Closed-form expressions of the Asymptotic CRB (ACRB) for the COLD-ULA

4.1. Definition of the Asymptotic CRB (ACRB)

In this paper, term "asymptotic" refers to the deterministic CRB considered for a large number of sensors,[3] *i.e.*, $L \gg 1$. In this case, we define the Asymptotic CRB for a COLD-ULA according to

$$\text{ACRB}^{(\text{COLD})}(\boldsymbol{\varepsilon}') \overset{\text{def}}{=} \left\{ \text{CRB}^{(\text{COLD})}(\boldsymbol{\varepsilon}') \text{ subject to } L \gg 1 \right\}$$

where $\text{CRB}^{(\text{COLD})}(\boldsymbol{\varepsilon}')$ is the CRB defined in (8)–(10). As the $\text{ACRB}^{(\text{COLD})}$ is essentially a CRB, this bound also satisfies the covariance inequality principle subject to $L \gg 1$. Note that this assumption seems severe but we will show in the simulation part that this constraint can be relaxed in practice.

4.2. Derivation of the lower bound

In Appendix A, we have reported the partial derivatives *wrt.* the model parameters of the vectorized noise-free model.

4.2.1. Example of the derivation of two blocks of the FIM

We first derive the $M \times M$ block of the FIM regarding the direction parameter defined by

---

[3] In other works, as for instance in [26], term "asymptotic" refers to the analysis of the CRB in the large Signal to Noise Ratio regime.

$$\boldsymbol{J_{\underline{\theta\theta}}} = \begin{bmatrix} \boldsymbol{J_{\theta_1\theta_1}} & \cdots & \boldsymbol{J_{\theta_1\theta_M}} \\ \vdots & & \vdots \\ \boldsymbol{J_{\theta_M\theta_1}} & \cdots & \boldsymbol{J_{\theta_M\theta_M}} \end{bmatrix} \tag{11}$$

where the (m, k)-th entry of the above matrix is

$$\boldsymbol{J_{\theta_m\theta_k}} = \frac{4\pi^2 d^2}{\lambda^2} \cos(\theta_m)\cos(\theta_k)$$

$$\times \sum_{t=1}^T \Re\{\boldsymbol{d_m'}^H(\boldsymbol{I_L} \otimes (\alpha_m^*(t)\boldsymbol{u_m^H}))(\boldsymbol{I_L} \otimes (\alpha_m(t)\boldsymbol{u_m}))\boldsymbol{d_m'}\}$$

$$+ \sum_{t=1}^T \Re\left\{ \frac{2i\pi d}{\lambda} \cos(\theta_m)\boldsymbol{d_m'}^H(\boldsymbol{I_L} \otimes (\alpha_m^*(t)\boldsymbol{u_m^H})) \right.$$

$$\left. \times \left(\boldsymbol{I_L} \otimes \left(\alpha_k(t)\frac{\partial \boldsymbol{u_k}}{\partial \theta_k} \right) \right) \boldsymbol{d_k} \right\}$$

$$+ \sum_{t=1}^T \Re\left\{ \frac{2i\pi d}{\lambda} \cos(\theta_k)\boldsymbol{d_m^H}\left(\boldsymbol{I_L} \otimes \left(\alpha_m^*(t)\frac{\partial \boldsymbol{u_m}^H}{\partial \theta_m} \right) \right) \right.$$

$$\left. \times (\boldsymbol{I_L} \otimes (\alpha_k(t)\boldsymbol{u_k}))\boldsymbol{d_k'} \right\}$$

$$+ \sum_{t=1}^T \Re\left\{ \boldsymbol{d_m^H}\left(\boldsymbol{I_L} \otimes \left(\alpha_m^*(t)\frac{\partial \boldsymbol{u_m}}{\partial \theta_m} \right) \right) \right.$$

$$\left. \times \left(\boldsymbol{I_L} \otimes \left(\alpha_k(t)\frac{\partial \boldsymbol{u_k}}{\partial \theta_k} \right) \right) \boldsymbol{d_k} \right\}$$

$$= \frac{4T\pi^2 d^2 \cos(\theta_m)\cos(\theta_k)}{\lambda^2} \Re\left\{ \langle\boldsymbol{d_m'}, \boldsymbol{d_k'}\rangle \hat{r}_{mk}\langle\boldsymbol{u_m}, \boldsymbol{u_k}\rangle \right\}$$

$$+ \frac{2T\pi d \cos(\theta_m)}{\lambda} \Re\left\{ i\langle\boldsymbol{d_m'}, \boldsymbol{d_k}\rangle \hat{r}_{mk}\left\langle \boldsymbol{u_m}, \frac{\partial \boldsymbol{u_k}}{\partial \theta_k} \right\rangle \right\} \tag{12}$$

$$+ \frac{2T\pi d \cos(\theta_k)}{\lambda} \Re\left\{ i\langle\boldsymbol{d_m}, \boldsymbol{d_k'}\rangle \hat{r}_{mk}\left\langle \frac{\partial \boldsymbol{u_m}}{\partial \theta_m}, \boldsymbol{u_k} \right\rangle \right\}$$

$$+ T\Re\left\{ \langle\boldsymbol{d_m}, \boldsymbol{d_k}\rangle \hat{r}_{mk}\left\langle \frac{\partial \boldsymbol{u_m}}{\partial \theta_m}, \frac{\partial \boldsymbol{u_k}}{\partial \theta_k} \right\rangle \right\} \tag{13}$$

$$= \frac{4T\pi^2 d^2 \cos(\theta_m)\cos(\theta_k)}{\lambda^2} \Re\left\{ \langle\boldsymbol{d_m'}, \boldsymbol{d_k'}\rangle \hat{r}_{mk}\langle\boldsymbol{u_m}, \boldsymbol{u_k}\rangle \right\}$$

in which $(.)^*$ stands for the conjugate,

$$\boldsymbol{d_m'} = \begin{bmatrix} 0 & e^{\frac{2i\pi d}{\lambda}\sin(\theta_m)} & 2e^{\frac{4i\pi d}{\lambda}\sin(\theta_m)} & \cdots & (L-1)e^{\frac{2i\pi d(L-1)}{\lambda}\sin(\theta_m)} \end{bmatrix}^T$$

and $\hat{r}_{mk} = \frac{1}{T}\sum_{t=1}^T \alpha_m^*(t)\alpha_k(t) = \frac{a_m a_k}{T}\sum_{t=1}^T e^{i(\phi_k(t)-\phi_m(t))}$ is the sample correlation coefficient of the sources. In the above expression, we used P1., $\frac{\partial \boldsymbol{u_k}}{\partial \theta_k} = \boldsymbol{0}$. Now, consider that we dispose of a large number of sensors *i.e.*, $L \gg 1$, we have [24,38]:

$$\frac{1}{L^3}\langle\boldsymbol{d_k'}, \boldsymbol{d_m'}\rangle \overset{L\gg 1}{\longrightarrow} \frac{1}{3}\delta_{k-m}, \qquad \frac{1}{L^2}\langle\boldsymbol{d_k'}, \boldsymbol{d_m}\rangle \overset{L\gg 1}{\longrightarrow} \frac{1}{2}\delta_{k-m},$$

$$\frac{1}{L}\langle\boldsymbol{d_k}, \boldsymbol{d_m}\rangle \overset{L\gg 1}{\longrightarrow} \delta_{k-m}$$

where δ_{k-m} is the Kronecker symbol defined by $\delta_{k-m} = 1$ for $k = m$ and zero otherwise. In this scenario, expression (13) can be simplified to

$$\boldsymbol{J_{\theta_m\theta_k}} \overset{L\gg 1}{\longrightarrow} \frac{4Td^2\pi^2 \cos^2(\theta_m)}{\lambda^2} \frac{L^3}{3} \Re\left\{ \hat{r}_{mk}\langle\boldsymbol{u_m}, \boldsymbol{u_k}\rangle \right\} \delta_{k-m}. \tag{14}$$

We can see that $\boldsymbol{J}_{\underline{\theta\theta}}$ is a diagonal matrix. So, for $m = k$, the sample correlation coefficient is $\hat{r}_{mm} = a_m^2$ and $\|\boldsymbol{u}_m\|^2 = 1$ (see P2.). As a consequence, (14) becomes

$$\boldsymbol{J}_{\underline{\theta\theta}} \xrightarrow{L \gg 1} \frac{4\pi^2 T d^2 L^3}{3\lambda^2} \boldsymbol{\Delta}^2 \boldsymbol{\Theta}^2 \tag{15}$$

where $\boldsymbol{\Theta} = \mathrm{diag}\{\cos(\theta_1), \ldots, \cos(\theta_M)\}$ and $\boldsymbol{\Delta} = \mathrm{diag}\{a_1, \ldots, a_M\}$. Remark that the sources can be correlated and the number of snapshots does not need to be large. Next we derive the block expressions of the FIM for the time-varying phase of the source. First, we have

$$\boldsymbol{J}_{\phi_m(t)\phi_k(t')}$$
$$= \begin{cases} 0 & \text{for } t \neq t', \\ a_m a_k \Re\{e^{i(\phi_k(t) - \phi_m(t))} \langle \boldsymbol{d}_m, \boldsymbol{d}_k \rangle \langle \boldsymbol{u}_m, \boldsymbol{u}_k \rangle\} & \text{otherwise.} \end{cases}$$

Note that, the time-diversity of the model implies that $\boldsymbol{J}_{\underline{\phi\phi}}$ is block-diagonal. This property is true for any L. In the asymptotic regime ($L \gg 1$), each of these blocks becomes diagonal since

$$\boldsymbol{J}_{\phi_m(t)\phi_k(t')} \xrightarrow{L \gg 1} \begin{cases} L a_m^2 & \text{for } t = t' \text{ and } m = k, \\ 0 & \text{for } t = t' \text{ and } k \neq m, \\ 0 & \text{for } t \neq t', \end{cases}$$

and thus

$$\boldsymbol{J}_{\underline{\phi}(t)\underline{\phi}(t')} = \begin{bmatrix} \boldsymbol{J}_{\phi_1(t)\phi_1(t')} & \cdots & \boldsymbol{J}_{\phi_M(t)\phi_M(t')} \\ \vdots & & \vdots \\ \boldsymbol{J}_{\phi_M(t)\phi_1(t')} & \cdots & \boldsymbol{J}_{\phi_M(t)\phi_M(t')} \end{bmatrix}_{M \times M}$$
$$\xrightarrow{L \gg 1} \begin{cases} L \boldsymbol{\Delta}^2, & \text{for } t = t', \\ \boldsymbol{0}, & \text{otherwise.} \end{cases}$$

Using the above expressions, we obtain

$$\boldsymbol{J}_{\underline{\phi\phi}} = \begin{bmatrix} \boldsymbol{J}_{\underline{\phi}(1)\underline{\phi}(1)} & \cdots & \boldsymbol{J}_{\underline{\phi}(1)\underline{\phi}(T)} \\ \vdots & & \vdots \\ \boldsymbol{J}_{\underline{\phi}(T)\underline{\phi}(1)} & \cdots & \boldsymbol{J}_{\underline{\phi}(T)\underline{\phi}(T)} \end{bmatrix}_{(TM) \times (TM)}$$
$$\xrightarrow{L \gg 1} L (\boldsymbol{I}_T \otimes \boldsymbol{\Delta}^2).$$

4.2.2. Final expressions of the other blocks of the FIM

Using a similar method as in the previous section and after some tedious derivations, we obtain

$$\boldsymbol{J}_{\underline{\theta\psi}} \xrightarrow{L \gg 1} \left(\frac{-iT\pi dL^2}{\lambda} \right) \boldsymbol{\Delta}^2 \boldsymbol{\Theta} \boldsymbol{\mathcal{D}}^H \boldsymbol{\mathcal{D}}_{\underline{\psi}},$$
$$\boldsymbol{J}_{\underline{\theta\phi}} \xrightarrow{L \gg 1} \left(\frac{\pi dL^2}{\lambda} \right) \left[\boldsymbol{\Delta}^2 \boldsymbol{\Theta} \quad \cdots \quad \boldsymbol{\Delta}^2 \boldsymbol{\Theta} \right]_{M \times (TM)}, \tag{16}$$

$$\boldsymbol{J}_{\underline{\psi\psi}} \xrightarrow{L \gg 1} (TL) \boldsymbol{\Delta}^2 \boldsymbol{\mathcal{D}}_{\underline{\psi}}^H \boldsymbol{\mathcal{D}}_{\underline{\psi}},$$
$$\boldsymbol{J}_{\underline{\psi\phi}} \xrightarrow{L \gg 1} (L\,i) \left[\boldsymbol{\Delta}^2 \boldsymbol{\mathcal{D}}_{\underline{\psi}}^H \boldsymbol{\mathcal{D}} \quad \cdots \quad \boldsymbol{\Delta}^2 \boldsymbol{\mathcal{D}}_{\underline{\psi}}^H \boldsymbol{\mathcal{D}} \right], \tag{17}$$

$$\boldsymbol{J}_{\underline{aa}} \xrightarrow{L \gg 1} (TL) \boldsymbol{I}_M, \qquad \boldsymbol{J}_{\underline{\rho\rho}} \xrightarrow{L \gg 1} (TL) \boldsymbol{\Delta}^2. \tag{18}$$

To obtain the above expressions, we used P2. and P3. ($\|\boldsymbol{u}_m\|^2 = \|\partial \boldsymbol{u}_m / \partial \rho_m\|^2 = 1$) and introduced the two block-diagonal matrices: $\boldsymbol{\mathcal{D}} = \mathrm{Bdiag}\{\boldsymbol{u}_1, \ldots, \boldsymbol{u}_M\}$ and $\boldsymbol{\mathcal{D}}_{\underline{\psi}} = \mathrm{Bdiag}\{\frac{\partial \boldsymbol{u}_1}{\partial \psi_1}, \ldots, \frac{\partial \boldsymbol{u}_M}{\partial \psi_M}\}$. In addition, we have $\boldsymbol{J}_{\underline{\rho a}} = \boldsymbol{J}_{\underline{a\rho}} = \boldsymbol{0}_{M \times M}$ and $\boldsymbol{J}_{\underline{\phi\rho}} = \boldsymbol{0}_{(TM) \times M}$, using P4., i.e., $\langle \boldsymbol{u}_m, \partial \boldsymbol{u}_m / \partial \rho_m \rangle = 0$ and $\boldsymbol{J}_{\underline{\theta a}}, \boldsymbol{J}_{\underline{\psi\rho}}, \boldsymbol{J}_{\underline{\psi a}} \xrightarrow{L \gg 1} \boldsymbol{0}_{M \times M}$ and $\boldsymbol{J}_{\underline{\phi a}} \xrightarrow{L \gg 1} \boldsymbol{0}_{(TM) \times M}$. Since all these quantities are asymptotically pure imaginary complex, they vanish by considering the real part in definition (10).

4.2.3. Block-diagonal FIM

Finally, using the results given in the two previous paragraphs, the FIM is asymptotically block-diagonal and has the following particular structure

$$\boldsymbol{F}_{\boldsymbol{\varepsilon}'\boldsymbol{\varepsilon}'} \xrightarrow{L \gg 1} L \begin{bmatrix} \boldsymbol{A} & \boldsymbol{0} \\ \boldsymbol{0} & \bar{\boldsymbol{A}} \end{bmatrix} \tag{19}$$

where the north-west block of size $(M(T+2)) \times (M(T+2))$ is given by the sparse band matrix given in Box I.

The south-west block of size $(2M) \times (2M)$ is the following diagonal matrix:

$$\bar{\boldsymbol{A}} = T \begin{bmatrix} \boldsymbol{\Delta}^2 & \boldsymbol{0} \\ \boldsymbol{0} & \boldsymbol{I}_M \end{bmatrix}.$$

$$\boldsymbol{A} = \boldsymbol{V} \boldsymbol{\Pi} \boldsymbol{V} \tag{20}$$

where

$$\boldsymbol{\Pi} = \begin{bmatrix} \frac{4T\pi^2 d^2 L^2}{3\lambda^2} \boldsymbol{\Theta}^2 & \left(\frac{-iT\pi dL}{\lambda} \right) \boldsymbol{\Theta} \boldsymbol{\mathcal{D}}^H \boldsymbol{\mathcal{D}}_{\underline{\psi}} & \left(\frac{\pi dL}{\lambda} \right) \boldsymbol{\Theta} & \cdots & \left(\frac{\pi dL}{\lambda} \right) \boldsymbol{\Theta} \\ \left(\frac{iT\pi dL}{\lambda} \right) \boldsymbol{\Theta} \boldsymbol{\mathcal{D}}_{\underline{\psi}}^H \boldsymbol{\mathcal{D}} & T \boldsymbol{\mathcal{D}}_{\underline{\psi}}^H \boldsymbol{\mathcal{D}}_{\underline{\psi}} & i\boldsymbol{\mathcal{D}}_{\underline{\psi}}^H \boldsymbol{\mathcal{D}} & \cdots & i\boldsymbol{\mathcal{D}}_{\underline{\psi}}^H \boldsymbol{\mathcal{D}} \\ \left(\frac{\pi dL}{\lambda} \right) \boldsymbol{\Theta} & -i\boldsymbol{\mathcal{D}}^H \boldsymbol{\mathcal{D}}_{\underline{\psi}} & \boldsymbol{I}_M & & \boldsymbol{0} \\ \vdots & \vdots & & \ddots & \\ \left(\frac{\pi dL}{\lambda} \right) \boldsymbol{\Theta} & -i\boldsymbol{\mathcal{D}}^H \boldsymbol{\mathcal{D}}_{\underline{\psi}} & \boldsymbol{0} & & \boldsymbol{I}_M \end{bmatrix}$$

and

$$\boldsymbol{V} = \boldsymbol{I}_{T+2} \otimes \boldsymbol{\Delta}.$$

Box I.

It is worth noting that considering large L implies a strongly structured FIM.

4.2.4. Analytic inverse of the FIM and closed-form expressions of the ACRB

Considering the remarkable block-structure of the FIM in (19), finding an analytic inverse of the FIM is equivalent to finding the analytic expressions of $\boldsymbol{A}^{-1}$ and $\bar{\boldsymbol{A}}^{-1}$. An analytic inverse of the factorized matrix (20) can be easily obtained. Indeed, we have $\boldsymbol{A}^{-1} = \boldsymbol{V}^{-1}\boldsymbol{\Pi}^{-1}\boldsymbol{V}^{-1}$ where $\boldsymbol{V}^{-1} = \boldsymbol{I}_{T+2} \otimes \boldsymbol{\Delta}^{-1}$. Before calculating the inverse of FIM, it is necessary to analyze the non-singularity of $\boldsymbol{A}$, by calculating its determinant. Applying in expression (20) the fact that the determinant of the product is the product of the determinants, we must verify that

$$\det\{\boldsymbol{A}\} = \det\{\boldsymbol{\Pi}\}\det\{\boldsymbol{V}\}^2 = \det\{\boldsymbol{\Pi}\}\prod_{m=1}^{M}a_m^{2(T+2)} \neq 0. \quad (21)$$

As we assumed that $a_m \neq 0$, we have to show that $\boldsymbol{\Pi}$ is nonsingular. Let define the following partition $\boldsymbol{\Pi} = \begin{bmatrix} \boldsymbol{\Pi}_{11} & \boldsymbol{\Pi}_{12} \\ \boldsymbol{\Pi}_{12}^H & \boldsymbol{\Pi}_{22} \end{bmatrix}$ where $\boldsymbol{\Pi}_{22} = \boldsymbol{I}_{MT}$. The definition of the other blocks can be easily deduced. Using a well-known expression of the determinant of a block matrix, we obtain

$$\det\{\boldsymbol{\Pi}\} = \det\{\boldsymbol{\Pi}_{22}\}\det\{\boldsymbol{Q}\} \quad (22)$$

where $\boldsymbol{Q}$ is the $(2M) \times (2M)$ Schur complement [39,40] defined by

$$\boldsymbol{Q} = \boldsymbol{\Pi}_{11} - \boldsymbol{\Pi}_{12}\boldsymbol{\Pi}_{22}^{-1}\boldsymbol{\Pi}_{12}^H \quad (23)$$

such that $\boldsymbol{\Pi}^{-1} = \begin{bmatrix} \boldsymbol{Q}^{-1} & \times \\ \times & \times \end{bmatrix}$. Note that matrix $\boldsymbol{\Pi}_{22}$ is a non-singular matrix ($\det\{\boldsymbol{\Pi}_{22}\} = 1$), so relation (23) is well defined. Consequently, relation (22) becomes

$$\det\{\boldsymbol{\Pi}\} = \det\{\boldsymbol{Q}\}. \quad (24)$$

Following definition (23), a simple derivation of the Schur complement leads to the following diagonal matrix:

$$\boldsymbol{Q} = T \begin{bmatrix} \dfrac{\pi^2 L^2 d^2}{3\lambda^2}\boldsymbol{\Theta}^2 & \boldsymbol{0} \\ \boldsymbol{0} & \boldsymbol{\mathcal{D}}_{\underline{\psi}}^H\boldsymbol{\mathcal{P}}_{\boldsymbol{\mathcal{D}}}^{\perp}\boldsymbol{\mathcal{D}}_{\underline{\psi}} \end{bmatrix} \quad (25)$$

where $\boldsymbol{\mathcal{P}}_{\boldsymbol{\mathcal{D}}}^{\perp} = \text{Bdiag}\{\boldsymbol{\mathcal{P}}_1^{\perp}, \ldots, \boldsymbol{\mathcal{P}}_M^{\perp}\}$, with $\boldsymbol{\mathcal{P}}_m^{\perp} = \boldsymbol{I}_2 - \boldsymbol{u}_m\boldsymbol{u}_m^H$ a rank-1 orthogonal projector onto the linear subspace $\langle\boldsymbol{u}_m\rangle^{\perp}$ and $\boldsymbol{\mathcal{D}}_{\underline{\psi}}^H\boldsymbol{\mathcal{P}}_{\boldsymbol{\mathcal{D}}}^{\perp}\boldsymbol{\mathcal{D}}_{\underline{\psi}} = \text{diag}\left\{\left\|\boldsymbol{\mathcal{P}}_1^{\perp}\frac{\partial\boldsymbol{u}_1}{\partial\psi_1}\right\|^2, \ldots, \left\|\boldsymbol{\mathcal{P}}_M^{\perp}\frac{\partial\boldsymbol{u}_M}{\partial\psi_M}\right\|^2\right\}$. Now, remark $\left\|\boldsymbol{\mathcal{P}}_m^{\perp}\frac{\partial\boldsymbol{u}_m}{\partial\psi_m}\right\|^2 = \left\|\frac{\partial\boldsymbol{u}_m}{\partial\psi_m}\right\|^2 - \left|\langle\frac{\partial\boldsymbol{u}_m}{\partial\psi_m}, \boldsymbol{u}_m\rangle\right|^2$ provides a direct link to the largest canonical principal angle [41,42], Ψ_m, between the two one-dimensional linear spaces $\langle\boldsymbol{u}_m\rangle$ and $\langle\frac{\partial\boldsymbol{u}_m}{\partial\psi_m}\rangle$ defined by

$$\sin^2(\Psi_m) = 1 - \frac{\left|\langle\frac{\partial\boldsymbol{u}_m}{\partial\psi_m}, \boldsymbol{u}_m\rangle\right|^2}{\left\|\frac{\partial\boldsymbol{u}_m}{\partial\psi_m}\right\|^2}. \quad (26)$$

Using P5. and P6., we have $\left|\langle\frac{\partial\boldsymbol{u}_m}{\partial\psi_m}, \boldsymbol{u}_m\rangle\right| = \left\|\frac{\partial\boldsymbol{u}_m}{\partial\psi_m}\right\|^2 = \sin^2(\rho_m)$. Thus, an interesting characterization of the

largest canonical angle can be obtained by rewriting expression (26) according to

$$\sin^2(\Psi_m) = 1 - \frac{\sin^4(\rho_m)}{\sin^2(\rho_m)} = \cos^2(\rho_m). \quad (27)$$

As $\Psi_m, \rho_m \in [0, \pi/2]$ and based on the above relation, we have

$$\Psi_m = \pi/2 - \rho_m. \quad (28)$$

Thus, the largest canonical angle is completely characterized by the polarization parameter ρ_m. Finally, we have

$$\boldsymbol{\mathcal{D}}_{\underline{\psi}}^H\boldsymbol{\mathcal{P}}_{\boldsymbol{\mathcal{D}}}^{\perp}\boldsymbol{\mathcal{D}}_{\underline{\psi}} = \boldsymbol{R}^2\boldsymbol{\Psi}^2 \quad (29)$$

where $\boldsymbol{R} = \text{diag}\{\sin(\rho_1), \ldots, \sin(\rho_M)\}$ and $\boldsymbol{\Psi} = \text{diag}\{\sin(\Psi_1), \ldots, \sin(\Psi_M)\} = \text{diag}\{\cos(\rho_1), \ldots, \cos(\rho_M)\}$. Using the diagonal structure of the Schur complement, the determinant of matrix $\boldsymbol{\Pi}$ using expression (24) is given by

$$\det\{\boldsymbol{Q}\} \propto \det\{\boldsymbol{\Theta}^2\}\det\{\boldsymbol{R}^2\boldsymbol{\Psi}^2\}$$
$$\propto \prod_{m=1}^{M}\cos^2(\theta_m)\sin^2(\rho_m)\cos^2(\rho_m) \quad (30)$$

where symbol $\propto$ means *proportional to*. Thus, to verify $\det\{\boldsymbol{Q}\} \neq 0$, the following three conditions must be satisfied:

1. $\theta_m \neq \pi/2$. This means (see Fig. 1) that the sources must not have DOAs perpendicular to the array. Such a source would produce a zero phase-shift between any two COLD pairs, its DOA being thus unobservable by the array.

2. $\rho_m \neq 0$ (*i.e.*, $\Psi_m \neq \pi/2$). This means (see Section 2 and Fig. 2) that linear horizontal polarizations are not allowed. Such a polarization would excite only the loops of the COLD array, and would be impossible to observe by the dipoles.

3. $\rho_m \neq \pi/2$ (*i.e.*, $\Psi_m \neq 0$). This means (see Section 2 and Fig. 2) that linear vertical polarizations are not allowed, either. Such a polarization would excite only the dipoles of the COLD array, and would be impossible to observe by the loops.

All the cases enumerated above would induce a FIM matrix that is singular. Adding the assumption that $a_m \neq 0$, we can conclude that under the above four conditions, the inverse of matrix $\boldsymbol{A}$ is given by Eq. (31) in Box II, thanks to the well-known geometric equality $\sin(2\rho_m) = 2\sin(\rho_m)\cos(\rho_m)$. Considering the diagonal terms of the above matrix up to $\sigma^2/(2L)$, we obtain:

$$\text{ACRB}^{(\text{COLD})}(\theta_m) = \frac{3\sigma^2}{2TL^3a_m^2}\frac{\lambda^2}{\pi^2 d^2\cos^2(\theta_m)}, \quad (32)$$

$$\text{ACRB}^{(\text{COLD})}(\psi_m) = \frac{2\sigma^2}{TLa_m^2}\frac{1}{\sin^2(2\rho_m)}. \quad (33)$$

It remains to derive the ACRB$^{(\text{COLD})}$ for the polarization parameters $\{\rho_1, \ldots, \rho_M\}$. Firstly remark that $\bar{\boldsymbol{A}}$ is nonsingular if $\det\{\bar{\boldsymbol{A}}\} \propto \prod_{m=1}^{M}a_m^2 \neq 0$. As, we have assumed that

$$\boldsymbol{A}^{-1} = \frac{1}{T} \begin{bmatrix} \frac{3\lambda^2}{\pi^2 L^2 d^2} \boldsymbol{\Theta}^{-2} \boldsymbol{\Delta}^{-2} & \times & \times & \times & \times \\ \times & \frac{4}{\sin^2(2\rho_1)} \boldsymbol{\Delta}^{-2} & & \boldsymbol{0} & \times \\ \times & & \ddots & & \times \\ \times & \boldsymbol{0} & & \frac{4}{\sin^2(2\rho_M)} \boldsymbol{\Delta}^{-2} & \times \\ \times & \times & \times & \times & \times \end{bmatrix} \tag{31}$$

<p style="text-align:center">**Box II.**</p>

that the real amplitudes are non-zeros, this condition is always verified. The inverse the north-west block of $\bar{\boldsymbol{A}}$ is simply $\frac{1}{T}\boldsymbol{\Delta}^{-2}$. Considering the diagonal terms up to $\sigma^2/(2L)$ (see (8) and (19)), we finally find:

$$\text{ACRB}^{(\text{COLD})}(\rho_m) = \frac{\sigma^2}{2TLa_m^2}. \tag{34}$$

5. Analysis of the ACRB for COLD-ULA

5.1. Remarks and properties

1. The $\text{ACRB}^{(\text{COLD})}$ regarding the direction parameter is anisotropic since the $\text{ACRB}^{(\text{COLD})}(\theta_m)$ depends of θ_m. This is also true and well-known for the uniformly polarized ULA [43].
2. The $\text{ACRB}^{(\text{COLD})}(\theta_m)$ is not a function of the polarization parameters. The intuitive reason for that is the fact that the magnetic loops are insensitive to the source azimuth angles. As the sources are all localized in the azimuthal plane, the polarization vector $\mathbf{u}_m$ in (3) and the localization parameter θ_m are fully decoupled.

   However, for elevation angles different from $\pi/2$, this result does not hold anymore. A formal proof for that is not straightforward since the analytic CRB for all elevation-DOAs is arduous to derive.
3. The $\text{ACRB}^{(\text{COLD})}(\psi_m)$ is a function of the polarization parameter ρ_m. The inverse is not true.
4. The $\text{ACRB}^{(\text{COLD})}(\psi_m)$ is sensitive to the geometry of the polarization state vector and its derivative with respect to parameter ψ_m. The lowest value that the bound $\text{ACRB}^{(\text{COLD})}(\psi_m)$ can reach is $\frac{2\sigma^2}{TLa_m^2}$ for $\rho_m = \pi/4$. This means [33] that the polarization ellipse orientation angle $\beta = \frac{\pi}{4}$ or the ellipticity $\alpha = \frac{\pi}{4}$ (circular polarization). Both cases imply that the dipoles and the loops are equally excited by the impinging source. The worst performance scenario corresponds to $\rho_m = 0$ (linear horizontal polarization) or $\rho_m = \frac{\pi}{2}$ (linear vertical polarization), in which cases only the loops or only the dipoles, respectively, are excited by the impinging wave.

   However, even in the favorable case, the polarization parameter ρ_m is better estimated than the polarization parameter ψ_m as $\text{ACRB}^{(\text{COLD})}(\psi_m) > \text{ACRB}^{(\text{COLD})}(\rho_m)$, regardless of the parameter values (see (33) and (34)).
5. All the bounds are function of the inverse of the local Signal to Noise Ratio (a_m^2/σ^2).

6. The $\text{ACRB}^{(\text{COLD})}$ for the localization parameter is in $O(1/L^3)$ while the $\text{ACRB}^{(\text{COLD})}$ for the polarization parameters are simply in $O(1/L)$. This means that the estimation of the DOAs is much more sensitive to the number of sensors than the estimation of the polarization parameters.

5.2. The known polarization state vector case

Consider the bound, denoted by $\text{ACRB}^{(\text{COLD})}(\theta_m | \underline{\psi}, \underline{\rho})$, where we assume that the polarization state is known. Considering a known polarization state implies that the polarization parameters in vector $\boldsymbol{\varepsilon}'$ are removed according to $\boldsymbol{\varepsilon}'' = \boldsymbol{P}\boldsymbol{\varepsilon}'$ with $\boldsymbol{P}$ a convenient $(M(T+2)) \times (M(T+4))$ selection matrix. This produces a reduced-size FIM, $\boldsymbol{F}_{\boldsymbol{\varepsilon}''\boldsymbol{\varepsilon}''}$, which shares the same block-structure as $\boldsymbol{F}_{\boldsymbol{\varepsilon}'\boldsymbol{\varepsilon}'}$. Focusing only on block $\boldsymbol{A}$, there exists a selection matrix $\boldsymbol{P}_0$ of size $(M(T+1)) \times (M(T+2))$, extracted from the larger matrix $\boldsymbol{P}$, such as

$$\boldsymbol{A}_0 \overset{\text{def}}{=} \boldsymbol{P}_0 \boldsymbol{A} \boldsymbol{P}_0^T = (\boldsymbol{I}_{T+1} \otimes \boldsymbol{\Delta})\boldsymbol{\Pi}_0(\boldsymbol{I}_{T+1} \otimes \boldsymbol{\Delta})$$

where $\boldsymbol{\Pi}_0$ can be easily deduced. The key point is that the $(2M) \times (2M)$ Schur complement derived for matrix $\boldsymbol{\Pi}$ in expression (25) can be linked to the $M \times M$ Schur complement of $\boldsymbol{\Pi}_0$ according to $\boldsymbol{Q}^{-1} = \begin{bmatrix} \bar{\boldsymbol{Q}}^{-1} & \times \\ \times & \times \end{bmatrix}$. Thus, compared to expression (25), we have $\bar{\boldsymbol{Q}}^{-1} = \frac{3\lambda^2}{\pi^2 TL^2 d^2} \boldsymbol{\Theta}^{-2}$ and thus

$$\text{ACRB}^{(\text{COLD})}(\theta_m | \underline{\psi}, \underline{\rho}) = \text{ACRB}^{(\text{COLD})}(\theta_m).$$

The result is somewhat unexpected and means that the estimation accuracy of the localization parameter is the same, regardless the knowledge of the polarization state.

5.3. Localization with a COLD-ULA compared to the uniformly polarized ULA

Denote by $\text{ACRB}(\theta_m)$ the ACRB for a uniformly polarized ULA, derived in Appendix B. The number of unknown model parameters (direction parameter, amplitude and phase of the source) in the $\text{ACRB}(\theta_m)$ is $M(T+2)$ while the number of the unknown model parameters in the $\text{ACRB}^{(\text{COLD})}(\theta_m)$ is higher (equal to $M(T+4)$). Therefore, a direct comparison between these two bounds is unfair. However, if we consider the case (studied in the previous subsection) of a COLD-ULA where the polarization parameters are known, then the two bounds, $\text{ACRB}(\theta_m)$

and ACRB$^{(\text{COLD})}(\theta_m|\underline{\psi}, \underline{\rho})$, have the same number of unknown parameters. Comparing expressions (32) and (B.4), we can readily check that

$$\text{ACRB}^{(\text{COLD})}(\theta_m) = \text{ACRB}(\theta_m).$$

This means that with a COLD-ULA, more model parameters can be estimated than with a uniformly polarized ULA, without degrading the estimation accuracy of the localization parameter.

5.4. The case of known complex sources

In this section, we study the ACRB$^{(\text{COLD})}$ when the complex sources in model (3) are *a priori* known. This scenario is relevant for some particular applications. For instance, in wireless communications the complex sources are perfectly known at the receiver in case of using a set of training sequences (see [44,45] for instance). Thus, the complex sources are no longer desired parameters and we define the unknown model parameters by

$$\boldsymbol{\varepsilon}''' \overset{\text{def}}{=} [\underline{\theta}^T, \underline{\psi}^T, \underline{\rho}^T]^T.$$

We denote by ACRB$^{(\text{COLD})}(\boldsymbol{\varepsilon}'''|\underline{\phi}, \underline{a})$ the ACRB for a COLD-ULA array when vectors $\underline{\phi}$ of initial phases and $\underline{a}$ of real amplitudes are *a priori* known. We have ACRB$^{(\text{COLD})}(\boldsymbol{\varepsilon}'''|\underline{\phi}, \underline{a}) = \frac{\sigma^2}{2}\boldsymbol{F}_{\boldsymbol{\varepsilon}'''\boldsymbol{\varepsilon}'''}^{-1}$ where $\boldsymbol{F}_{\boldsymbol{\varepsilon}'''\boldsymbol{\varepsilon}'''}$ is the new FIM with respect to vector $\boldsymbol{\varepsilon}'''$. There exists a $(3M) \times (M(T+4))$ selection matrix $\boldsymbol{W}$ such that $\boldsymbol{\varepsilon}''' = \boldsymbol{W}\boldsymbol{\varepsilon}'$, where $\boldsymbol{\varepsilon}'$ was defined in (7). Thus, matrix $\boldsymbol{W}$ removes from $\boldsymbol{\varepsilon}'$ the known parameters (real amplitudes and initial phases). In this case, we have

$$\boldsymbol{F}_{\boldsymbol{\varepsilon}'''\boldsymbol{\varepsilon}'''} = \boldsymbol{W}\boldsymbol{F}_{\boldsymbol{\varepsilon}'\boldsymbol{\varepsilon}'}\boldsymbol{W}^T$$

$$= LT \left[\begin{array}{cc|c} \frac{4\pi^2 d^2 L^2}{3\lambda^2}\boldsymbol{\Delta}^2\boldsymbol{\Theta}^2 & \left(\frac{\pi dL}{\lambda}\right)\boldsymbol{\Delta}^2\boldsymbol{\Theta}\boldsymbol{R}^2 & \boldsymbol{0} \\ \hline \left(\frac{\pi dL}{\lambda}\right)\boldsymbol{\Delta}^2\boldsymbol{\Theta}\boldsymbol{R}^2 & \boldsymbol{\Delta}^2\boldsymbol{R}^2 & \boldsymbol{0} \\ \hline \boldsymbol{0} & \boldsymbol{0} & \boldsymbol{\Delta}^2 \end{array} \right] \quad (35)$$

since $\boldsymbol{\mathcal{D}}^H\boldsymbol{\mathcal{D}}_{\underline{\psi}} = i\boldsymbol{R}^2$ and $\boldsymbol{\mathcal{D}}_{\underline{\psi}}^H\boldsymbol{\mathcal{D}}_{\underline{\psi}} = \boldsymbol{R}^2$.

5.4.1. The direction parameter

The Schur complement of the above matrix is given by $\boldsymbol{\mathcal{Q}} = \frac{\pi^2 L^3 d^2 T}{3\lambda^2}\boldsymbol{\Delta}^2\boldsymbol{\Theta}^2(\boldsymbol{I} + 3\boldsymbol{\Psi}^2)$. A simple derivation yields

$$\text{ACRB}^{(\text{COLD})}(\theta_m|\underline{\phi}, \underline{a}) = G_m \, \text{ACRB}^{(\text{COLD})}(\theta_m)$$

where $G_m = \frac{1}{1+3\cos^2(\rho_m)}$. As $\rho_m \in (0, \pi/2)$, we have $G_m \leq 1$ (see Fig. 3) and therefore

$$\text{ACRB}^{(\text{COLD})}(\theta_m|\underline{\phi}, \underline{a}) \leq \text{ACRB}^{(\text{COLD})}(\theta_m).$$

As intuitively expected, integrating prior-knowledge on the sources can decrease the ACRB$^{(\text{COLD})}(\theta_m)$. We can say that according to Fig. 3, if parameter ρ_m is close to $\pi/2$ (the polarization is close to linear vertical), the ACRB$^{(\text{COLD})}(\theta_m)$ is close to the ACRB$^{(\text{COLD})}(\theta_m|\underline{\phi}, \underline{a})$ and thus the accuracy estimation for the direction parameter is weakly improved in the case of known sources. Inversely, for polarizations
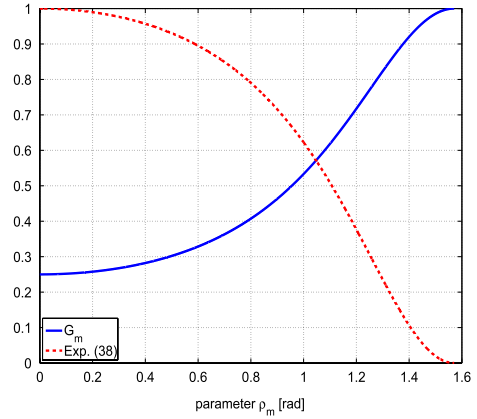
Fig. 3. Ratio G_m and expression (38) Vs. parameter ρ_m.

close to linear horizontal, *i.e.* ρ_m close to zero, the accuracy estimation for the DOA parameter can be considerably improved by taking into account information on the source signals.

5.4.2. The polarization parameters

The $(2, 2)$-th block of the inverse of the FIM provides the bound for the parameter $\underline{\psi}$ according to

$$\text{ACRB}^{(\text{COLD})}(\underline{\psi}|\underline{\phi}, \underline{a})$$

$$= \frac{\sigma^2}{2TL}\left(\boldsymbol{\Delta}^{-2}\boldsymbol{R}^{-2} + 3(\boldsymbol{I} + \boldsymbol{\Delta}^{-2}(\boldsymbol{I} + 3\boldsymbol{\Psi})^{-1})\right) \quad (36)$$

or equivalently for the m-th parameter,

$$\text{ACRB}^{(\text{COLD})}(\psi_m|\underline{\phi}, \underline{a})$$

$$= \frac{\sigma^2}{2TLa_m^2\sin^2(\rho_m)}\left(1 + \frac{3\sin^2(\rho_m)}{1 + 3\cos^2(\rho_m)}\right)$$

$$= \frac{2\sigma^2 G_m}{TLa_m^2\sin^2(\rho_m)}. \quad (37)$$

It comes the following interesting relation

$$\frac{\text{ACRB}^{(\text{COLD})}(\psi_m|\underline{\phi}, \underline{a})}{\text{ACRB}^{(\text{COLD})}(\psi_m)} = 4\cos^2(\rho_m)G_m. \quad (38)$$

According to Fig. 3, we have

$$\text{ACRB}^{(\text{COLD})}(\psi_m|\underline{\phi}, \underline{a}) \leq \text{ACRB}^{(\text{COLD})}(\psi_m).$$

Here again, integrating the prior-knowledge of the sources can decrease the ACRB$^{(\text{COLD})}$. We can say that according to Fig. 3, if the polarization is close to linear horizontal (ρ_m is close to zero), the ACRB$^{(\text{COLD})}(\psi_m)$ is close to the ACRB$^{(\text{COLD})}(\psi_m|\underline{\phi}, \underline{a})$. On the contrary, for values of ρ_m close to $\frac{\pi}{2}$ (polarization close to linear vertical), the prior-knowledge of the sources allows to better estimate parameter ψ_m.

Regarding the polarization parameter ρ_m, we have

$$\text{ACRB}^{(\text{COLD})}(\rho_m|\underline{\phi}, \underline{a}) = \text{ACRB}^{(\text{COLD})}(\rho_m).$$

6. Numerical analysis of the bound

We consider a COLD-ULA with $L = 13$ sensors with half-wavelength inter-spacing sensors. Two narrowband far-field sources ($M = 2$) are located according to $\theta_1 = -70°$ and $\theta_2 = 10°$ with unit real amplitudes ($a_1 = a_2 = 1$). The polarization state is parametrized by $\rho_1 = 60°$, $\rho_2 = 15°$, $\psi_1 = 5°$ and $\psi_2 = 15°$.

6.1. Relative Squared Error

The CRB$^{(\text{COLD})}$ is computed for the direction and polarization parameters by a numerical evaluation and inversion of the FIM and compared to the proposed ACRB$^{(\text{COLD})}$. On Fig. 4(a), we have drawn the Relative Squared Error (RSE) defined by

$$\text{RSE}(\theta_1) = \frac{|\text{CRB}^{(\text{COLD})}(\theta_1) - \text{ACRB}^{(\text{COLD})}(\theta_1)|^2}{|\text{CRB}^{(\text{COLD})}(\theta_1)|^2}$$

for the direction parameter θ_1, for $T = 100$ snapshots and for a fixed noise variance ($\sigma^2 = 1$). The RSE(ψ_1) and RSE(ρ_1) are accordingly introduced and drawn in Fig. 4(b) and (c), respectively. The RSE has a nice property given by

$$0 < \text{RSE}(.) < 1.$$

This can be shown by noting that ACRB$^{(\text{COLD})}(.) > 0$, thus CRB$^{(\text{COLD})}(.) - \text{ACRB}^{(\text{COLD})}(.) < \text{CRB}^{(\text{COLD})}(.)$. Considering the squared absolute value, one gets

$$|\text{CRB}^{(\text{COLD})}(.) - \text{ACRB}^{(\text{COLD})}(.)|^2 < |\text{CRB}^{(\text{COLD})}(.)|^2.$$

This means that the approximation error by considering the ACRB$^{(\text{COLD})}$ *wrt.* the CRB$^{(\text{COLD})}$ is higher bounded by the CRB$^{(\text{COLD})}$, itself. It is well-known that at high SNR and for not too closely-spaced sources, the CRB$^{(\text{COLD})}$ takes a small value. This means that the approximation error is small.

According to Fig. 4(b) and (c), we can see that the decrease of the RSE with respect to the number of sensors for the direction and polarization parameters is given by

$$\text{RSE}(\theta_1), \text{RSE}(\psi_1), \text{RSE}(\rho_1) \sim O(1/L^4).$$

In addition, we can also note that even for a small of number of sensors, as for instance 13 sensors, the RSE is small since RSE(θ_1) $\approx 10^{-3}$, RSE(ψ_1) $\approx 10^{-4}$ and RSE(ρ_1) $\approx 10^{-4}$. From a practical point of view, this means that the asymptotic assumption is not severe and the asymptotic regime is rapidly reached for sufficiently spaced sources. Remark that a similar observation has been done in [30]. According to Fig. 5, we can see that even for a moderate number of sensors, all the ACRB$^{(\text{COLD})}$ are very close to their corresponding CRB$^{(\text{COLD})}$, for sufficiently spaced sources. We can verify that the ACRB$^{(\text{COLD})}$ for the direction parameter is identical to the ACRB$^{(\text{COLD})}$ for the same parameter with known polarization state (see Section 5.2). We also verify the result derived in Section 5.4 for the case where the complex sources are known.

It is also interesting to plot (see Fig. 6(a)) the RSE *wrt.* the proximity of the sources. We can see that the RSE is maximal (close to one) if the sources are very close. In this scenario, the ACRB$^{(\text{COLD})}$ is not a consistent approximation of the CRB$^{(\text{COLD})}$. Nevertheless, if the constraint of proximity of the sources is relaxed, the ACRB$^{(\text{COLD})}$ becomes a valid approximation of the CRB$^{(\text{COLD})}$ (see Fig. 6(b)).
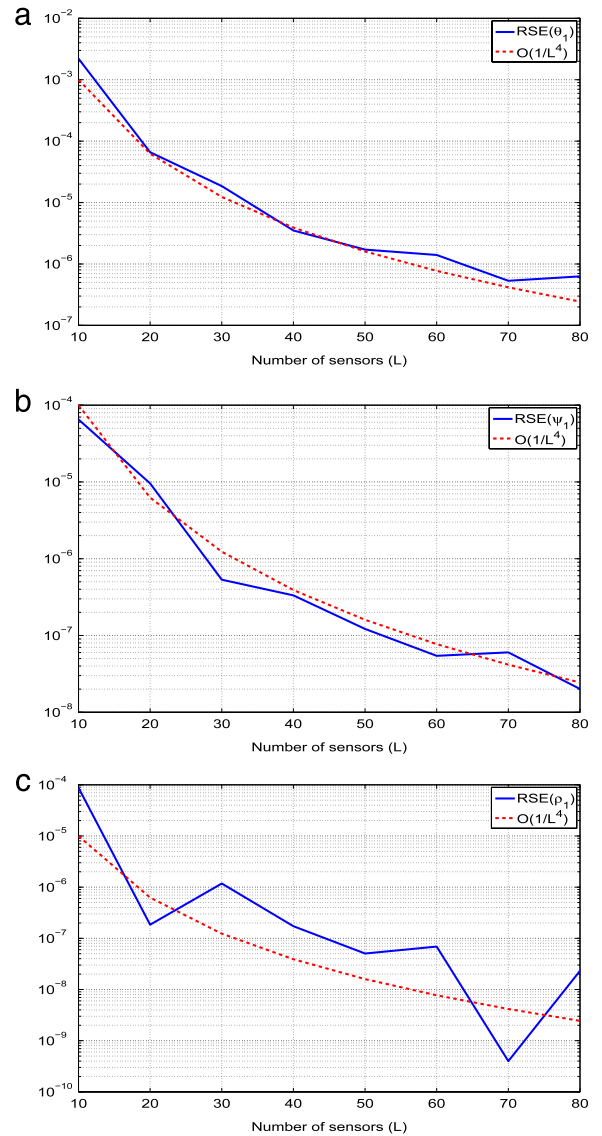
Fig. 4. RSE Vs. the number of sensors for (a) the direction parameter θ_1, (b) the angle ψ_1 and (c) the angle ρ_1 with $T = 100$ snapshots ($\sigma^2 = 1$).

6.2. Asymptotic numerical diagonality of the block of the FIM regarding the direction parameter

Consider on Fig. 7, an error metric relatively to the diagonal term of $\mathbf{J}_{\underline{\theta\theta}}$ defined by

$$E_{mk}(L) = (|\mathbf{J}_{\theta_m\theta_k} - \boldsymbol{\mathcal{J}}_{\theta_m\theta_k}|^2)/|\mathbf{J}_{\theta_m\theta_m}|^2$$

where $\mathbf{J}_{\theta_m\theta_k} \xrightarrow{L \gg 1} \boldsymbol{\mathcal{J}}_{\theta_m\theta_k}$. For $m \neq k$ (*resp.* $m = k$), we consider the error on the off-diagonal (*resp.* diagonal) terms relatively to the diagonal ones for matrix $\mathbf{J}_{\underline{\theta\theta}}$. Thus, this metric characterizes the "asymptotic numerical diagonality" of $\mathbf{J}_{\underline{\theta\theta}}$. This metric decreases in $O(1/L^2)$ and is small even for a small/moderate number of sensors (see Fig. 7). For instance, consider 13 sensors, $E_{mk}(L) = |\mathbf{J}_{\theta_m\theta_k}|^2/|\mathbf{J}_{\theta_m\theta_m}|^2 \approx 6 \cdot 10^{-3}$ meaning that the off-diagonal terms are strongly dominated by the diagonal ones. For the
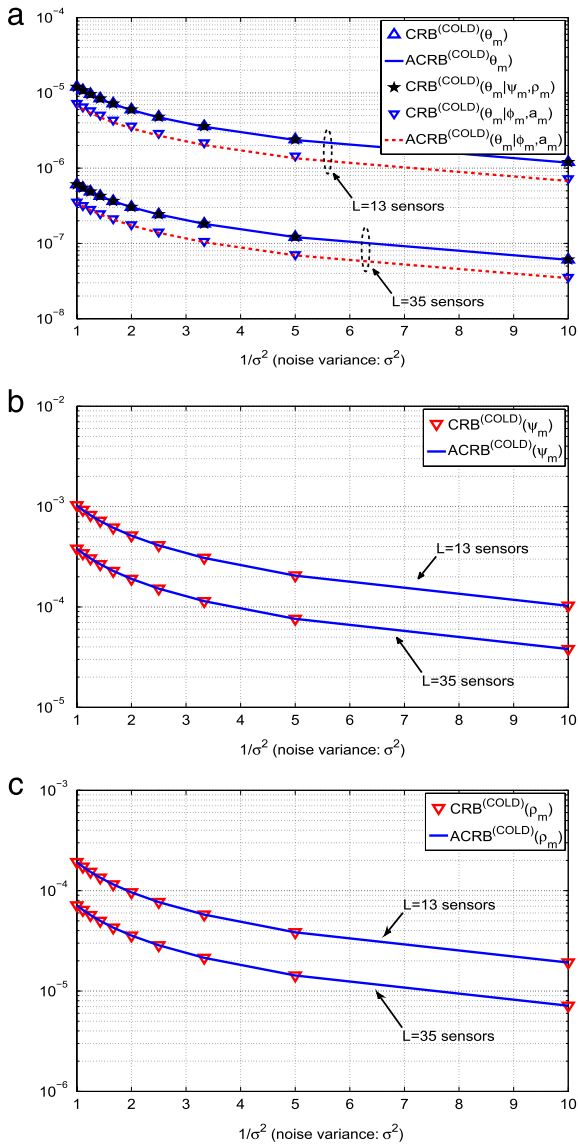
Fig. 5. Estimation accuracy for the COLD array in log-scale Vs. the noise variance with $T = 50$ snapshots.

same number of sensors, we have $E_{mm}(L) \approx 10^{-2}$ which is also relatively small. From a practical point of view, this means that the asymptotic assumption can be relaxed.

7. Conclusion

In this work, we have studied the performance of the estimation of the direction and polarization parameters for a COLD-ULA in the case where the sources are all localized in the azimuthal plane. Toward this end, we have derived closed-form (nonmatrix) expressions of the deterministic CRB under the assumption that the number of sensors is sufficiently large. We show that this assumption is not severe in practice and the closed-form expressions are accurate for a number of sensors slightly higher than ten when the sources are widely-spaced. As a by product, it
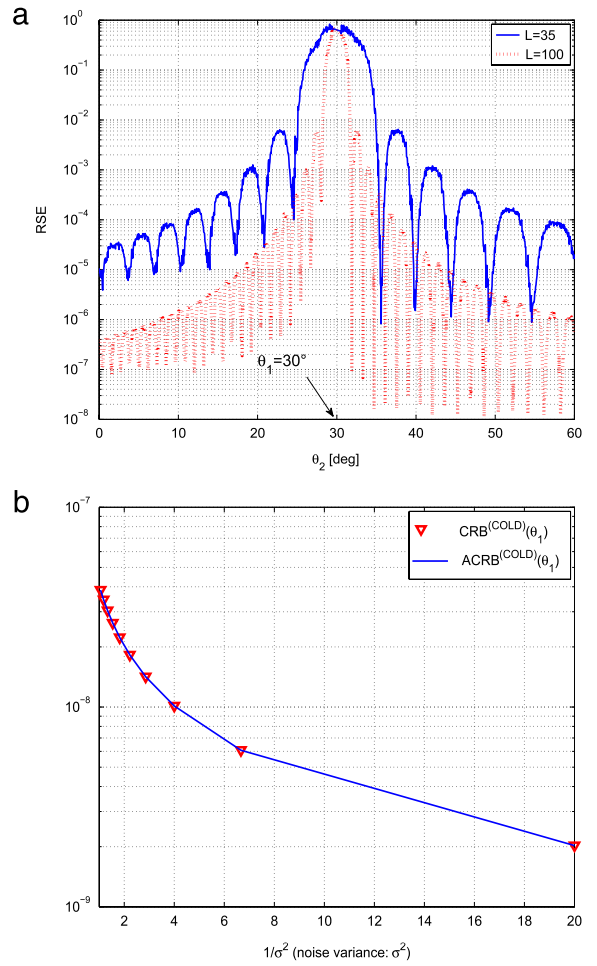
Fig. 6. (a) RSE for several number of sensors *wrt.* the proximity of the sources, (b) $\mathrm{CRB}^{(\mathrm{COLD})}(\theta_1)$ and $\mathrm{ACRB}^{(\mathrm{COLD})}(\theta_1)$ for $\theta_1 = 30°$ and $\theta_1 = 35°$ for $L = 35$.
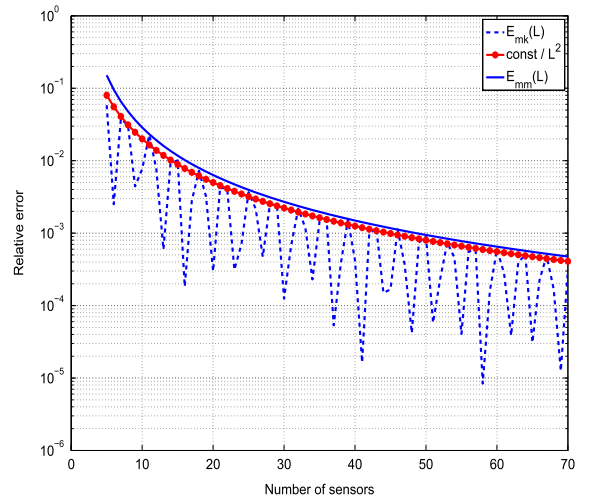
Fig. 7. Relative error of the diagonal and off-diagonal terms of matrix $\boldsymbol{J}_{\theta\theta}$ with $T = 100$ snapshots.

results a very cheap way to compute the deterministic CRB while the brute force computation of this lower bound needs to inverse a large FIM for $T \gg 1$. The main contribution of this work is the analysis of the proposed bound. More precisely, we prove that the accuracy of the direction parameter estimation is not affected whether the polarization state vector is known or not. This allows a fair comparison between the ACRB for a COLD-ULA and for an uniformly polarized ULA, since these two bounds have the same number of unknown model parameters. Finally, we show that with a COLD-ULA, more model parameters can be estimated than with the uniformly polarized ULA, without degrading the estimation accuracy of localization parameter. We also quantify precisely the interest of considering known complex sources, as it is sometimes the case in some applications as for instance in wireless communications.

Appendix A. Partial derivative vectors of the model *wrt.* the model parameters

We use intensively the first partial derivative of the model *wrt.* the model parameters. We provide these expressions in this Appendix:

$$\frac{\partial \check{\boldsymbol{x}}}{\partial \theta_m} = \frac{2i\pi d}{\lambda} \cos(\theta_m) \begin{bmatrix} (\boldsymbol{I}_L \otimes (\alpha_m(1)\boldsymbol{u}_m)) \, \boldsymbol{d}'_m \\ \vdots \\ (\boldsymbol{I}_L \otimes (\alpha_m(T)\boldsymbol{u}_m)) \, \boldsymbol{d}'_m \end{bmatrix},$$

$$\frac{\partial \check{\boldsymbol{x}}}{\partial \psi_m} = \begin{bmatrix} \left(\boldsymbol{I}_L \otimes \left(\alpha_m(1)\frac{\partial \boldsymbol{u}_m}{\partial \psi_m}\right)\right) \boldsymbol{d}_m \\ \vdots \\ \left(\boldsymbol{I}_L \otimes \left(\alpha_m(T)\frac{\partial \boldsymbol{u}_m}{\partial \psi_m}\right)\right) \boldsymbol{d}_m \end{bmatrix},$$

$$\frac{\partial \check{\boldsymbol{x}}}{\partial \phi_m(t)} = i \begin{bmatrix} 0 \\ \vdots \\ 0 \\ (\boldsymbol{I}_L \otimes (\alpha_m(t)\boldsymbol{u}_m)) \, \boldsymbol{d}_m \\ 0 \\ \vdots \\ 0 \end{bmatrix},$$

$$\frac{\partial \check{\boldsymbol{x}}}{\partial \rho_m} = \begin{bmatrix} \left(\boldsymbol{I}_L \otimes \left(\alpha_m(1)\frac{\partial \boldsymbol{u}_m}{\partial \rho_m}\right)\right) \boldsymbol{d}_m \\ \vdots \\ \left(\boldsymbol{I}_L \otimes \left(\alpha_m(T)\frac{\partial \boldsymbol{u}_m}{\partial \rho_m}\right)\right) \boldsymbol{d}_m \end{bmatrix},$$

$$\frac{\partial \check{\boldsymbol{x}}}{\partial a_m} = \begin{bmatrix} \left(\boldsymbol{I}_L \otimes (e^{i(2\pi f_0 + \phi_m(1))}\boldsymbol{u}_m)\right) \boldsymbol{d}_m \\ \vdots \\ \left(\boldsymbol{I}_L \otimes (e^{i(2\pi f_0 T + \phi_m(T))}\boldsymbol{u}_m)\right) \boldsymbol{d}_m \end{bmatrix}.$$

Appendix B. Derivation of the ACRB for an uniformly polarized ULA with multiple snapshots

The model parameters are collected in the following $((T+2)M) \times 1$ vector:

$$\boldsymbol{\varepsilon}'' = \begin{bmatrix} \underline{\theta}^T & \underline{\phi}^T & \underline{a}^T \end{bmatrix}^T.$$

The FIM for an ULA is given by

$$\bar{\boldsymbol{F}}_{\boldsymbol{\varepsilon}''\boldsymbol{\varepsilon}''} \xrightarrow{L \gg 1} L \begin{bmatrix} \boldsymbol{B} & \boldsymbol{0} \\ \boldsymbol{0} & T\boldsymbol{I}_M \end{bmatrix} \tag{B.1}$$

where

$$\boldsymbol{B} = \begin{bmatrix} \frac{4\pi^2 d^2 T L^2}{3\lambda^2}\boldsymbol{\Theta}^2\boldsymbol{\Delta}^2 & \frac{\pi dL}{\lambda}\boldsymbol{\Delta}^2\boldsymbol{\Theta} & \cdots & \frac{\pi dL}{\lambda}\boldsymbol{\Delta}^2\boldsymbol{\Theta} \\ \hline \frac{\pi dL}{\lambda}\boldsymbol{\Delta}^2\boldsymbol{\Theta} & \boldsymbol{\Delta}^2 & & \boldsymbol{0} \\ \vdots & & \ddots & \\ \frac{\pi dL}{\lambda}\boldsymbol{\Delta}^2\boldsymbol{\Theta} & \boldsymbol{0} & & \boldsymbol{\Delta}^2 \end{bmatrix}. \tag{B.2}$$

The inverse of the Schur complement [40,39] associated with matrix $\boldsymbol{B}$ is given by

$$\tilde{\boldsymbol{Q}}^{-1} = \frac{3\lambda^2}{\pi^2 d^2 T L^2}\boldsymbol{\Theta}^{-2}\boldsymbol{\Delta}^{-2} \tag{B.3}$$

with $\boldsymbol{B}^{-1} = \begin{bmatrix} \tilde{\boldsymbol{Q}}^{-1} & \times \\ \times & \times \end{bmatrix}$. Considering the diagonal terms of the above expression up to $\sigma^2/(2L)$, we obtain

$$\text{ACRB}(\theta_m) = \frac{3\sigma^2}{2TL^3 a_m^2} \frac{\lambda^2}{\pi^2 d^2 \cos^2(\theta_m)}. \tag{B.4}$$

References

[1] I. Ziskind, M. Wax, Maximum likelihood localization of diversely polarized sources by simulated annealing, IEEE Trans. Antennas and Propagation 38 (1990) 1111–1114.

[2] J. Li, Direction and polarization estimation using arrays with small loops and short dipoles, IEEE Trans. Antennas and Propagation 41 (1) (1993) 379–387.

[3] K.T. Wong, M.D. Zoltowski, Uni-vector-sensor esprit for multisource azimuth, elevation, and polarization estimation, IEEE Trans. Signal Process. 45 (10) (1997) 1467–1474.

[4] K.T. Wong, M.D. Zoltowski, Closed-form direction-finding with arbitrarily spaced electromagnetic vector-sensors at unknown locations, IEEE Trans. Antennas and Propagation 48 (5) (2000) 671–681.

[5] M.D. Zoltowski, K.T. Wong, ESPRIT-based 2D direction finding with a sparse array of electromagnetic vector-sensors, IEEE Trans. Signal Process. 48 (8) (2000) 2195–2204.

[6] D. Donno, A. Nehorai, U. Spagnolini, Seismic velocity/polarization estimation and polarized wavefield separation, IEEE Trans. Signal Process. (2008) 4794–4809.

[7] K.T. Wong, M.D. Zoltowski, Self-initiating MUSIC-based direction finding and polarization estimation in spatio-polarizational beamspace, IEEE Trans. Antennas and Propagation 48 (2000) 1235–1245.

[8] K.T. Wong, L. Li, M.D. Zoltowski, Root-MUSIC-based direction-finding and polarization-estimation using diversely-polarized possibly-collocated antennas, IEEE Antennas Wirel. Propag. Lett. 3 (8) (2004) 129–132.

[9] J. Li, P. Stoica, D. Zheng, Efficient direction and polarization estimation with a COLD array, IEEE Trans. Antennas and Propagation 44 (4) (1996) 539–547.

[10] A. Manikas, J.W. Peng, Crossed-dipole arrays for asynchronous DS-CDMA systems, IEEE Trans. Antennas and Propagation 45 (10) (1997) 1467–1474.

[11] S. Miron, N. Le Bihan, J. Mars, Vector-MUSIC for polarized seismic source localisation, EURASIP J. Applied Signal Process. 20 (1) (2005) 74–84.

[12] P. Chevalier, A. Ferreol, L. Albera, G. Birot, Higher order direction finding from arrays with diversely polarized antennas: the PD-2q-MUSIC algorithms, IEEE Trans. Signal Process. 55 (11) (2007) 5337–5350.

[13] S. Miron, N. Le Bihan, J.I. Mars, Quaternion MUSIC for vector-sensor array processing, IEEE Trans. Signal Process. 54 (4) (2006) 1218–1229.

[14] N. Le Bihan, S. Miron, J.I. Mars, MUSIC algorithm for vector-sensors array using biquaternions, IEEE Trans. Signal Process. 55 (9) (2007) 4523–4533.

[15] K.C. Ho, K.C. Tan, W. Ser, Investigation on number of signals whose directions-of-arrival are uniquely determinable with an electromagnetic vector sensor, Signal Process. 47 (1995) 41–54.

[16] B. Hochwald, A. Nehorai, Identifiability in array processing models with vector-sensor applications, IEEE Trans. Signal Process. 44 (1996) 83–95.

[17] X. Guo, S. Miron, D. Brie, S. Zhu, X. Liao, A CANDECOMP/PARAFAC perspective on uniqueness of DOA estimation using a vector sensor array, IEEE Trans. Signal Process. 59 (7) (2011) 3475–3481.

[18] M.N. El Korso, R. Boyer, A. Renaux, S. Marcos, Statistical resolution limit of the uniform linear cocentered orthogonal loop and dipole array, IEEE Trans. Signal Process. 59 (1) (2011) 425–431.

[19] A. Nehorai, E. Paldi, Vector-sensor array processing for electromagnetic source localization, IEEE Trans. Signal Process. 42 (2) (1994) 376–398.

[20] J. Li, P. Stoica, Efficient parameter estimation of partially polarized electromagnetic waves, IEEE Trans. Signal Process. 42 (1) (1994) 3114–3125.

[21] J. Lundback, S. Nordebo, Analysis of a tripole array for polarization and direction of arrival estimation, in: Sensor Array and Multichannel Signal Processing Workshop, 18–21 July 2004, pp. 284–288.

[22] J. Tabrikian, R. Shavit, D. Rahamim, An efficient vector sensor configuration for source localization, IEEE Signal Process. Lett. 11 (8) (2004) 690–693.

[23] A. Yeredor, On the role of constraints in system identification, in: IProc. of the 4th International Workshop on Total Least Squares and Errors-in-Variables Modeling, Arenbergcastle, Leuven, Belgium, August 21–23, 2006.

[24] P. Stoica, A. Nehorai, MUSIC, maximum likelihood, and Cramér–Rao bound, IEEE Trans. Signal Process. 37 (5) (1989) 720–741.

[25] P. Stoica, A. Nehorai, Performance study of conditional and unconditional direction-of-arrival estimation, IEEE Trans. Signal Process. 38 (10) (1990) 1783–1795.

[26] A. Renaux, P. Forster, E. Chaumette, P. Larzabal, On the high-SNR conditional maximum-likelihood estimator full statistical characterization, IEEE Trans. Signal Process. 54 (12) (2006) 4840–4843.

[27] B. Hochwald, A. Nehorai, Polarimetric modeling and parameter estimation with applications to remote sensing, IEEE Trans. Signal Process. 43 (8) (1995) 1923–1935.

[28] C.K.Au Yeung, K.T. Wong, Cramer–Rao bounds for estimation of pure-tone signals' azimuth-elevation arrival angles, polarization parameter and frequencies using a dipole-triad or a loop-triad, in: International Conference on Information, Communications and Signal Processing, vol. 2, 15–18 December 2003, pp. 1033–1037.

[29] C.K.Au Yeung, K.T. Wong, CRB: sinusoid-sources' estimation using collocated dipoles/loops, IEEE Trans. Aerosp. Electron. Syst. 45 (1) (2009) 94–109.

[30] P. Stoica, O. Besson, Training sequence design for frequency offset and frequency-selective channel estimation, IEEE Trans. Commun. 51 (11) (2003) 1910–1917.

[31] J.-P. Delmas, Closed-form expressions of the exact Cramer–Rao bound for parameter estimation of BPSK, MSK, or QPSK waveforms, IEEE Signal Process. Lett. 15 (2008) 405–408.

[32] E. Dilaveroglu, Nonmatrix Cramér–Rao bound expressions for high-resolution frequency estimators, IEEE Trans. Signal Process. 46 (2) (1998) 463–474.

[33] R.T. Compton, The tripole antenna: an adaptive array with full polarization flexibility, IEEE Trans. Antennas and Propagation AP-29 (6) (1981) 944–952.

[34] G.A. Deschamps, Geometrical representation of the polarization of a plane electromagnetic wave, Proc. IRE 39 (1951) 540–544.

[35] J. Li, R. Compton, Angle and polarization estimation using ESPRIT with a polarization sensitive array, IEEE Trans. Antennas and Propagation 39 (1991) 1376–1383.

[36] C.R. Rao, Information and accuracy attainable in the estimation of statistical parameters, Bull. Calcutta Math. Soc. 37 (1945) 81–91.

[37] H. Cramer, Mathematical Methods of Statistics, Princeton University Press, Princeton, NJ, 1946.

[38] I.S. Gradshteyn, I.M. Ryzhik, Table of Integrals, Series, and Products, Academic, New York, 1980.

[39] P. Stoica, R.L. Moses, Spectral Analysis of Signals, Prentice Hall, 2005.

[40] Z. Fuzhen, The Schur Complement and its Applications, in: Numerical Methods and Algorithms, vol. 4, Springer, 2005.

[41] G.H. Golub, C.F. Van Loan, Matrix Computations, 3rd ed., Johns Hopkins University Press, Baltimore, Maryland, 1996.

[42] L.L. Scharf, L.T. McWhorier, Geometry of the Cramer–Rao bound, Signal Process. 31 (2) (1993) 301–311.

[43] U. Baysal, R.L. Moses, On the geometry of isotropic arrays, IEEE Trans. Signal Process. 51 (6) (2003) 1469–1478.

[44] L.C. Godara, Application of antenna arrays to mobile communications, part II: beam-forming and direction-of-arrival considerations, Proc. IEEE 85 (8) (1997) 1195–1245.

[45] S. Buzzi, H.V. Poor, On parameter estimation in long-code DS/CDMA systems: Cramer–Rao bounds and least-squares algorithms, IEEE Trans. Signal Process. 51 (2) (2003) 545–559.

Rémy Boyer received the M.Sc. and the Ph.D. degrees in the field of signal processing and communications from Ecole Nationale Supérieure des Télécommunications (ENST) de Paris, France, in 1999 and 2002, respectively.

From 2002 to 2003, he was a Visiting Researcher at the University of Sherbrooke, QC, Canada. He is currently an Associate Professor at Laboratoire des Signaux et SystËmes (L2S), Gif-sur-Yvette with the CNRS-UPS-SUPELEC (National Center of Scientific Research and University of Paris-Sud XI). His research activities include multiway-arrays processing, sensor array and security in wireless network.

Sebastian Miron was born in Suceava, Romania, in 1977. He graduated from "Gh. Asachi" Technical University of Iasi, Romania, in 2001 and received the M.Sc. and the Ph.D. degree in signal, image, and speech processing from the Institut National Polytechnique of Grenoble, France, in 2002 and 2005, respectively.

He is currently a Maître de Conférence at Nancy-Université, France, and he is conducting research at the Centre de Recherche en Automatique de Nancy (CRAN), Nancy. His current research interests include vector-sensor array processing, positive source separation, multilinear algebra and hypercomplex numbers.